crystals

MDPI

Article

Weak Interactions in the Structures of Newly Synthesized (–)-Cytisine Amino Acid Derivatives

Anna K. Przybył *, Anita M. Grzeskiewicz and Maciej Kubicki *

Faculty of Chemistry, A. Mickiewicz University in Poznań, Uniwersytetu Poznańskiego 8, 61-614 Poznań, Poland; aniow@amu.edu.pl

* Correspondence: annaprz@amu.edu.pl (A.K.P.); mkubicki@amu.edu.pl (M.K.)

Abstract: Eight new (–)-(*N*-[(AA)-(*N*-phtaloyl)]cytisines (where AA is amino acid: glycine, β-alanine, *D*,*L*-valine, *L*-valine, *L*-isoleucine, *L*-leucine, *D*-leucine and *D*,*L*-phenyloalanine), were synthesized and fully spectroscopically characterized (NMR, FTIR and MS). For two of these compounds, *N*-[glycine-(*N*-phtaloyl)]cytisine and *N*-[*L*-isoleucine-(*N*-phtaloyl)]cytisine, X-ray crystal structures were obtained and used as the basis for an in-depth analysis of intermolecular interactions and packing energies. The structural geometrical data (weak hydrogen bonds, π···π interactions, etc.) were compared with the energies of interactions and the topological characteristics (electron density, Laplacian at the appropriate critical point) based on the atoms-in-molecules theory. The results suggest that there is no straightforward connection between the geometry of point-to-point interactions and the molecule-to-molecule energies. Additionally, the usefulness of the transfer of multipolar parameters in estimating of critical points' characteristics have been confirmed.

Keywords: alkaloid derivatives; weak interactions; weak hydrogen bonds; interaction energies; atoms-in-molecules topological analysis

Citation: Przybył, A.K.; Grzeskiewicz, A.M.; Kubicki, M. Weak Interactions in the Structures of Newly Synthesized (–)-Cytisine Amino Acid Derivatives. *Crystals* **2021**, *11*, 146. https://doi.org/10.3390/cryst11020146

Academic Editor: Magdalena Małecka

Received: 15 January 2021

Accepted: 26 January 2021

Published: 30 January 2021

1. Introduction

Intermolecular interactions are responsible for the aggregation of molecules into molecular crystals as well as into other larger moieties and in general into supramolecules [1]. This is the core of supramolecular chemistry, one of the most swiftly developing branches of chemistry, which found numerous applications in such different topics as molecular self-assembly, nanotechnology, catalysis, drug delivery and molecular switches (cf. e.g., [2]).

Therefore, systematical studies of intermolecular interactions are relevant for general chemistry, as well as for biology, material science, etc. Starting from "classical" hydrogen bonds of, e.g., O–H···O or O–H···N type, well-known for more than a century, the realm of such interactions expanded steadily to become a huge conglomerate of very different members, differing in their energies, geometries, nature, importance, etc. These include non-classical hydrogen bonds, for instance with C–H donors (which were the subject of fiery debate in the 1970s, e.g. [3]), with π–electron acceptors, etc., as well as halogen bonding [4], chalcogen bonding [5], pnicogen bonding [6], tetrel bonding [7], π···π interactions [8], cation···π interactions [9], anion···π interactions [10], etc. The huge variety of (more or less) real interactions makes it necessary to investigate their mutual importance, hierarchies and characteristics.

The aims for such studies include geometrical characteristics (distances, angles), most conveniently obtained by means of X-ray diffraction, energetic characteristics (interaction energies), which can be obtained by quantum-chemical calculations, topological characteristics (atoms-in-molecules description), etc. Here we present the results of such wide studies of intermolecular interactions in the crystal structures of two (–)-cytisine derivatives. A number of such derivatives was synthesized (Figure 1) and spectroscopically characterized, although for the sake of this study, two derivatives were picked

(*N*-[glycine-(*N*-phtaloyl)]cytisine (**3A**) and *N*-[*L*-isoleucine-(*N*-phtaloyl)]cytisine (**3E**)), because for these compounds we were able to obtain the crystals of quality appropriate for X-ray structural analysis. Additionally, we wanted to check the importance of the quality of the electron density model in estimating the critical points' characteristics, e.g., density at the critical point or the Laplacian value by comparing the values obtained for the standard X-ray determination with/without modifications, such as hydrogen position correction or multipolar parameters transfer with the results of high-resolution diffraction studies of similar compounds.

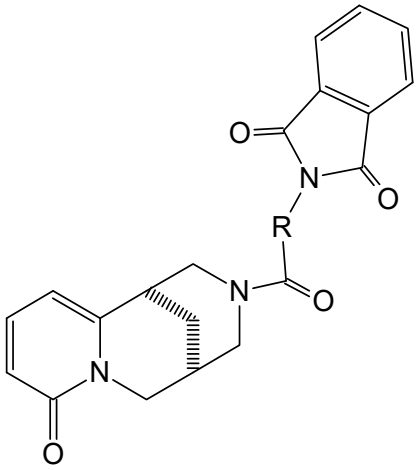

Figure 1. The structures of studied compounds. R = $–CH_2–$ (**3A**, *N*-[glycine-(*N*-phtaloyl)]cytisine), $–CH_2–CH_2–$ (**3B**, *N*-[β-alanine-(*N*-phtaloyl)]cytisine), $–CH(CH_3)_2–$ (**3C**, *N*-[*D*,*L*-valine-(*N*-phtaloyl)]cytisine), $–CH(CH_3)_2$ (**3D**, *N*-[*L*-valine-(*N*-phtaloyl)]cytisine), $–CH((CH_3)CH_2CH_3$ (**3E**, *N*-[*L*-isoleucine-(*N*-phtaloyl)]cytisine), $–CH_2CH(CH_3)_2$ (**3F**, *N*-[*L*-leucine-(*N*-phtaloyl)]cytisine), $–CH_2CH(CH_3)_2$ (**3G**, *N*-[*D*-leucine-(*N*-phtaloyl)]cytisine), $–CH_2C_6H_5$ (**3H**, *N*-[*D*,*L*-phenyloalanine-(*N*-phtaloyl)]cytisine).

(–)-Cytisine is a natural product, extracted from the plants of the Fabaceae (Leguminosae) family, and its importance stems from the fact that it has been found to have an affinity towards the specific subunits of nicotine acetylcholine receptors (nAChRs). The strongest nAChR agonists (receptor activators) are nicotine and epibatidine, which, however, due to their high toxicity, cannot be used in medical therapy [11]. Hence the increased importance of (–)-cytisine, which is a more selective ligand towards main nAChR receptors and less toxic than nicotine. Because of the similar mode of action and lower toxicity, (–)-cytisine **(1)** has been applied as a nicotine substitute in antinicotine therapy. (–)-Cytisine as a partial agonist of nAChR, and moderately increases the concentration of dopamine and thus alleviates the symptoms of nicotine withdrawal, the so-called nicotine craving. When administered together with nicotine, (–)-cytisine acts antagonistically towards nicotine, which reduces the receptor's response to the latter [12].

In the search for new ligands interacting with nicotine receptors, a number of (–)-cytisine derivatives have been obtained. The synthetic analogues of **(1)** have been mainly obtained by substitution of the nitrogen atom N–12 in ring C (ring names as in Scheme 1) and modification of the quasi-aromatic ring A [13]. In general, substitution at N-12 is considered as non-conducive to increasing affinity to receptors, but it is the simplest method to enhance the lipophilicity of (–)-cytisine, which increases the chances of its overcoming the blood–brain barrier. Due to the broad spectrum of effects, (**1**) is considered as a pharmacophoric block to conjugate with other synthetic or natural compounds. It has been proven that the linkers of different lengths and bioactivities are important factors in the effective design of new bioactive compounds. Additionally, it has been shown that the combination of two biological agents including cytisine and camphecene make a promising novel class of potential antiviral compounds [14].

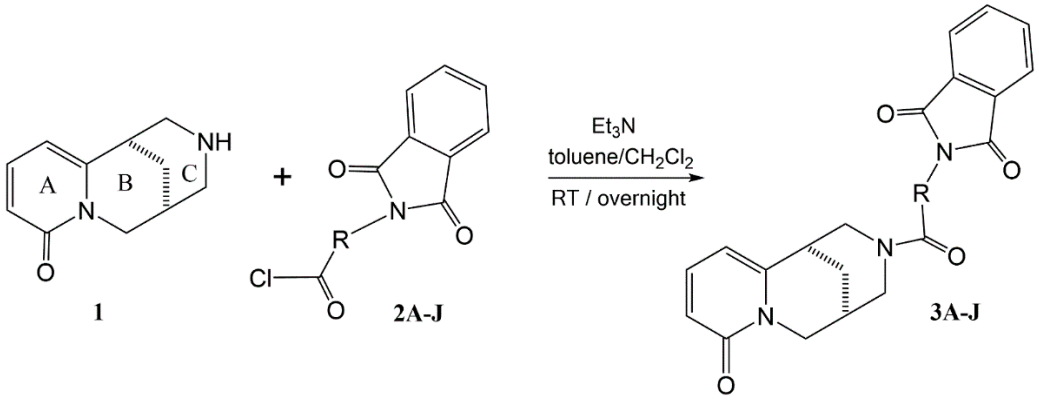

Scheme 1. Synthesis of new derivatives of cytisine (*N*-[amino acid-(*N*-phtaloyl)]cytisines, **3A–J**).

2. Materials and Methods

Flash chromatography was carried out on silica gel 60 G F254 (Merck). Melting points were determined on a Boetius apparatus (PHMK 05 VEB Wagetechnik Rapido, Radebeul). EIMS mass spectra were recorded using a model 402 two-sector mass spectrometer (AMD Intectra GmbH, Harpsted, Germany; ionizing voltage 70 eV, accelerating voltage 8 kV, resolution 1000 for low-resolution and 10 000 for high-resolution mass spectra). IR spectra were obtained on a FT-IR Bruker IFS 113v spectrometer (KBr pellets technique). NMR spectra were recorded on a Bruker AVANCE II 400 (400.13 MHz) spectrometer, with a 5 mm broadband probe head with actively shielded z gradient coil (90° ^{1}H pulse width 10.8 s, ^{13}C pulse width 12 μs.

2.1. Synthesis

General procedure for the synthesis of cytisine amino-acid derivatives (Figure 1 and Scheme 1):

A suitable amino acid with phthalic anhydride in a mortar in a 1:1 ratio were triturated. The ground reagents were transferred to a flask. For 1 hour, the substrates were melted in an oil bath at 150–160 °C under an argon atmosphere [15]. The resulting precipitate or oil was allowed to cool. The course of the reaction was monitored by TLC and developed in solution with ninhydrin to detect unreacted amino acid residues.

Blocked amino acids were treated with excess thionyl chloride (eq. 1:6.5). The mixture was cooled for about 30 minutes in an ice bath. Then the reagents were heated for 3 h [16]. The excess of thionyl chloride was removed on a rotary evaporator. The dissolved solid (in the case of compounds **2A**, **2B** and **2H**—the details in SI) or the yellow oil (in the case of compounds **2C**–**2G**—the details in SI) was dissolved in toluene to separate the product from insoluble impurities. The solvent was evaporated, and the product obtained was washed with warm hexane and left to dry [17]. Compound **2** was dissolved in a solution of CH_2Cl_2/toluene (2:1) and cooled in an ice bath. Then cytisine dissolved in the same solvent mixture was added (molar ratio 1:1). Next, 0.5 mL of triethylamine was added, and the reaction mixture was stirred overnight at room temperature [16]. The solvent was evaporated and the product purified on an Al_2O_3 column and washed out with CH_2Cl_2. The yield of the obtained compounds:

3A (*N*-[glycine-(*N*-phtaloyl)]cytisine), 97%; **3B** (*N*-[β-alanine-(*N*-phtaloyl)]cytisine), 54%; **3C** (*N*-[*D*,*L*-valine-(N-phtaloyl)]cytisine) 60%; **3D** (*N*-[*L*-valine-(*N*-phtaloyl)]cytisine), 69%; **3E** (*N*-[*L*-isoleucine-(*N*-phtaloyl)]cytisine), 58%; **3F** (*N*-[*L*-leucine-(*N*-phtaloyl)]cytisine), 89%; **3G** (*N*-[*D*-leucine-(*N*-phtaloyl)]cytisine), 60%; **3H** (*N*-[*D*,*L*-phenyloalanine-(*N*-phtaloyl)] cytisine), 47%.

Details of spectral analysis are submitted as Supplementary Information.

Mass Spectrometry: The degree of contamination of the products was evaluated on the basis of GC–MS, although this method did not permit detection of triethylamine and

its salt in the samples studied. Analysis of chromatograms provided the first information on the retention times (in Supplementary Information).

L-isomers were found to be characterized by longer R_t than their *D*-isomers, for example, for *D*-valine (**3C**) R_t = 43.336, while for *L*-valine (**3D**) R_t = 47.642 and in the case of *D*-leucine (**3G**) Rt = 51.099, and *L*-leucine (**3F**) R_t = 53.591 minutes. The obtained amino acid derivatives of cytisine were subjected to EI–MS examination [18,19], showing that molecular ions of the compounds studied, formed upon EI, undergo mass fragmentation in which the bonds at both sides of the carbonyl group break up, leading to formation of even-electron fragment ions **i** and **g** (Table 1, Scheme 2). Breaking up of a radical of the ion **g** structure from the molecular ion gives the ion **f**, which gives the ion **i** as a result of elimination of a CO molecule. The even-electron fragment ion **g** is the parent ion for two subsequent ions **j** and **m**. For the derivatives *L*-isoleucine (**3E**) and *L*-leucine (**3F**), we found that it is possible to distinguish between the two regio-isomers, as the spectrum of *L*-leucine (**3F**) differs from that of *L*-isoleucine (**3E**) by a higher relative abundance of the ions **d** and **l** (Table 1, Scheme 2).

Table 1. Elemental compositions and relative abundances of the ions in the EI spectra of compounds **3A**–**3H**.

Ion	Elemental Composition	m/z	3A	3B	3C (*D*)	3D (*L*)	3E (*L*)	3G (*D*)	3F (*L*)	3H (*D*)	3H (*L*)
$M^{+\bullet}$ **a**	$C_{21}H_{19}N_3O_4$	377 391	29	-	-	-	-	-	-	-	-
	$C_{22}H_{21}N_3O_4$			21	30	-	-	-	-	-	-
	$C_{24}H_{25}N_3O_4$	419	-	-	-	7	-	-	-	-	-
	$C_{25}H_{27}N_3O_4$	433	-	-	-	-	1	16	3	-	-
	$C_{28}H_{25}N_3O_4$	467	-							27	3
d	$C_{21}H_{19}N_3O_4$	377	-	-	4	12	70	34	46	-	-
f	$C_{12}H_{13}N_2O_2$	217	14	1	8	6	12	10	6	1	3
g	$C_9H_6NO_2$	160	100	-	-	-	-	-	-	30	13
	$C_{13}H_{14}NO_2$	216	-	-	-	-	19	24	41	-	-
	$C_{10}H_8NO_2$	174	-	5	-	-	-	-	-	13	1
	$C_{12}H_{12}NO_2$	202	-	-	100	100	-	-	-	2	-
i	$C_{11}H_{13}N_2O$	189	35	30	18	27	37	23	21	4	13
j	$C_9H_6NO_2$	160	100	73	63	67	100	100	100	30	13
l	$C_8H_5NO_2$	147	2	100	56	64	75	72	36	3	74
m	$C_8H_4NO_2$	146	87	81	64	58	55	54	36	35	38

The molecular ions (M^+) obtained for the compounds containing fragments of valine, leucine or isoleucine also undergoes decomposition involving elimination of $CH_2{=}C(CH_3)_2$ molecule, which leads to the ion at m/z 377 (Table 1, Scheme 2).

A detail analysis of EI–MS spectra (SI) permits distinction of stereoisomers *D* and *L*, present in the series of the analyzed compounds **3A–H**, just on the basis of relative abundances of selected fragmentation ions. In the spectra of stereoisomers *D* (**3C**-*D*; **3G**; **3H**-*D*, cytisine derivatives with valine or leucine) the relative intensity of the molecular ion (M^+) is higher and the fragmentation ion **d** is lower than the corresponding ones in the spectra of stereoisomers *L* (**3D**, **3F**, **3H**–*L*).

NMR spectra analysis. Amide conformers of cytisine derivatives occur in solutions in dynamic equilibrium [20,21]. Additionally, in the case of amino acid derivatives of cytisine, the presence of two cis and trans conformers is observed in ^{1}H NMR and ^{13}C NMR spectra (SI), which is recorded as a double set of signals. Each set corresponds to one of the two conformations of the analyzed compounds (Table 2).

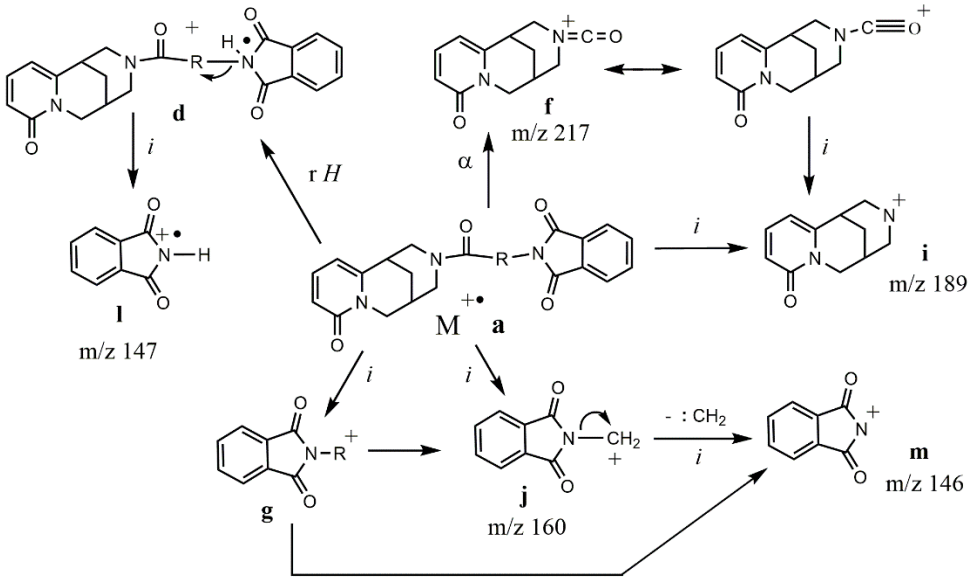

Scheme 2. Principal EI mass spectral fragmentation routes of compounds **3A–3H**.

Table 2. Chemical shifts δ (ppm) of carbon atoms of cytisine (^{13}C NMR in $CDCl_3$).

	1	**3A**	**3B**	**3D cis/trans**	**3E cis/trans**	**3F**	**3H**
At C				δ (ppm)			
2	162.26	165.1/164.6	163.6/163.5	163.2/162.4	163.3/162.4	162.9/162.9	162.9/162.9
3	115.04	118.3/117.7	117.4/116.9	117.3/116.9	117.3/116.8	117.9/117.3	118.1/117.2
4	138.64	138.8/138.4	139.5/139.1	139.0/136.8	139.0/136.9	138.6/137.4	137.0/136.8
5	103.80	105.6/104.7	106.6/105.9	105.8/104.0	105.8/104.1	105.1/104.3	105.9/105.1
6	152.34	147.7/147.7	148.4/148.2	134.2/131.4	148.1/148.1	147.9/147.9	134.1/133.9
7	34.68	34.8/34.1	34.7/34.0	27.6/26.8	33.3/32.9	30.0/29.6	35.2/34.3
8	25.78	26.1/25.9	25.71/25.6	20.8/20.0	26.1/25.9	24.9/24.8	26.1/25.9
9	27.13	27.3/27.3	27.2/27.0	26.7/26.2	27.6/26.7	27.2/27.0	27.4/26.8
10	49.39	48.7/48.7	49.9/48.5	49.4/48.9	51.5/51.1	49.2/48.7	51.7/51.3
11	52.53	49.4/48.3	48.4/47.5	51.3/51.0	48.9/48.5	50.6/50.2	48.748.7
13	53.45	52.3/50.9	52.7/51.43	55.8/55.3	54.7/54.3	51.6/51.6	51.7/51.3

X-ray diffraction. Diffraction data were collected by the ω-scan technique at room temperature on two Rigaku four-circle diffractometers: for **1** on XCalibur diffractometer with Sapphire2 CCD detector and graphite-monochromated MoK_α radiation (λ = 0.71069 Å), and for **2** on SuperNova with Atlas detector and mirror-monochromated CuK_α radiation (λ = 1.54178 Å). The data were corrected for Lorentz-polarization as well as for absorption effects [22]. Precise unit-cell parameters were determined by a least-squares fit of 2190 (**1**), and 11309 (**2**) reflections of the highest intensity, chosen from the whole experiment. The structures were solved with SHELXT-2013 [23] and refined with the full-matrix least-squares procedure on F^2 by SHELXL-2013 [24]. All non-hydrogen atoms were refined anisotropically, and hydrogen atoms were placed in idealized positions and refined as a "riding model" with isotropic displacement parameters set at 1.2 (1.5 for methyl groups) times U_{eq} of appropriate carrier atoms.

2.2. Crystal Data

1: $C_{21}H_{19}N_3O_4$, M_r = 377.39, orthorhombic, $P2_12_12_1$, a = 6.5691(6) Å, b = 12.2108(11) Å, c = 22.0780(16) Å, V = 1771.0(3) Å, Z = 4, d_x = 1.415 g·cm^{-3}, F(000) = 792 μ(MoK_α) = 0.100 mm^{-1}, 9310 reflections measured up to Θ = 26.91, 3505 symmetry-independent

(R_{int} = 2.99%), 2740 with = I > 2σ(I). Final R[I > 2σ(I)] = 4.10%, wR2[I > 2σ(I)] = 8.12%, R[all refl.] = 6.17%, wR2[all refl.] = 9.07%, S = 1.003, $\Delta\rho_{max}/\Delta\rho_{min}$ = 0.12/–0.16e·Å^{-3}.

2: $C_{25}H_{27}N_3O_4 \cdot CH_3CN$, M_r = 474.55, orthorhombic, $P2_12_12_1$, a= 7.26005(11) Å, b = 8.55757(14) Å, c = 39.3690(7) Å, V = 2445.93(7) Å, Z = 4, d_x = 1.289 g·cm^{-3}, F(000) = 1008 μ(CuK$_\alpha$) = 0.712 mm^{-1}, 22727 reflections measured up to Θ = 75.55, 4966 symmetry-independent (R_{int} = 5.95%), 4726 with I > 2σ(I). Final R[I > 2σ(I)] = 5.36%, wR2[I > 2σ(I)] = 15.21%, R[all refl.] = 5.57%, wR2[all refl.] = 15.38%, S=1.063, $\Delta\rho_{max}/\Delta\rho_{min}$ = 0.31/−0.16e·Å^{-3}.

Energy calculations. The calculations of interaction energies between pairs of molecules and packing energies were performed with two methods:

(a) Using wavefunctions at B3LYP/6-31G(d,p) level (hereinafter: B3LYP), the energy of interaction was calculated within the CrystalExplorer software [25] in terms of four key components: electrostatic, polarization, dispersion and exchange–repulsion $E_{tot} = k_{ele}E_{ele} + k_{pol}E_{pol} + k_{dis}E_{dis} + k_{rep}E_{rep}$

(b) and with the PIXEL method [26,27], as included in Mercury program [28].

In both cases the hydrogen atoms were moved to the average geometry as determined by neutron diffraction.

AIM topological analysis. The topology (atoms-in-molecules, [29]) of electron density distribution has been calculated using MoPro software [30].

3. Results and Discussion

Eight new (–)-(*N*-[AA-(N-phtaloyl)]cytisines were synthesized (cf. Figure 1). For two of them (**3A** (hereinafter **1**) and **3E** (**2**)) the crystal structures were determined, and the wide analysis of the structures and intermolecular interactions were performed. The comparison of the molecules shows that the overall conformations are radically different. Of course, in both two cases the cytisine moieties are rigid and the variations in their geometries are negligible, but the mutual orientation of the cytisine and phthalimide fragments is totally different. Figure 2 shows the comparison of two molecules with cytisine fragments fitted one onto another.

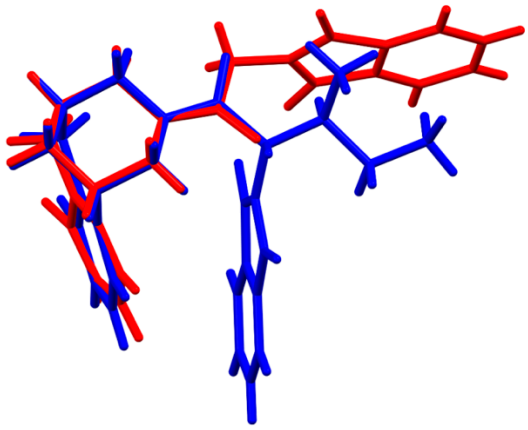

Figure 2. A comparison of conformations of **3A** (red) and **3E** (blue). The cytisine fragments were fitted one onto another.

In **3A** the ring A and phthalimide planes make an angle of 68.7°, while in **3E** these two planes are almost parallel, with dihedral angle of 14.0°. In this latter case intramolecular π-stacking (distance between the planes is ca. 3.7Å) might afford the additional factor stabilizing this conformation.

Figures 3 and 4 show the perspective views of the molecules **3A** and **3E**, respectively, and Table 3 lists the relevant geometrical parameters.

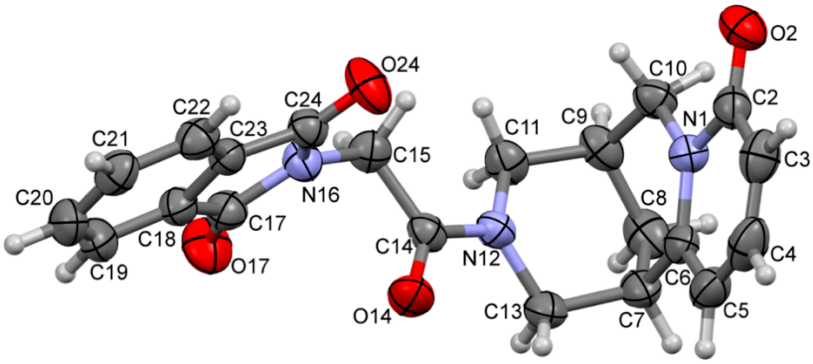

Figure 3. A perspective view of the molecule **3A**. Ellipsoids are drawn at the 50% probability level, hydrogen atoms are represented by spheres of arbitrary radii.

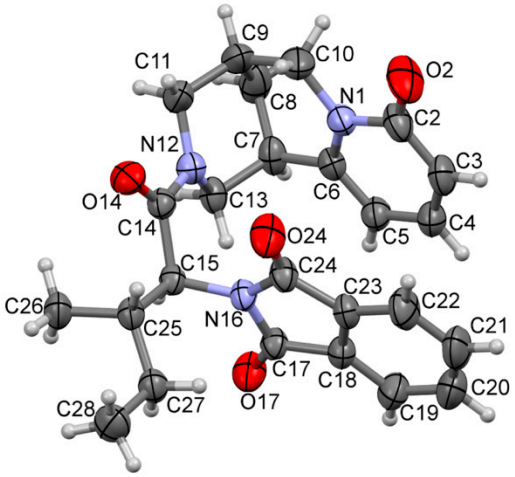

Figure 4. A perspective view of the molecule **3E.** Ellipsoids are drawn at the 50% probability level, hydrogen atoms are represented by spheres of arbitrary radii.

Table 3. Relevant geometric parameters (Å, °) with s.u.'s in parentheses.

	3A	3E		3A	3E
N1–C2	1.400(3)	1.418(4)	**N1–C6**	1.380(3)	1.369(4)
N1–C10	1.473(3)	1.478(5)	**C2–O2**	1.241(3)	1.241(5)
C11–N12	1.464(3)	1.463(4)	**N12–C13**	1.462(3)	1.461(4)
N12–C14	1.352(3)	1.364(4)	**C14–O14**	1.222(3)	1.218(4)
C15–N16	1.437(3)	1.470(4)	**N16–C17**	1.395(3)	1.397(4)
N16–C24	1.389(3)	1.406(4)	**C17–O17**	1.209(3)	1.199(4)
C24–O24	1.203(3)				
C2–N1–C6	122.4(2)	122.2(3)	**C2–N1–C10**	113.9(2)	114.1(3)
C6–N1–C10	123.7(2)	123.6(3)	**C11–N12–C13**	115.9(2)	114.6(3)
C11–N12–C14	123.6(2)	116.8(3)	**C13–N12–C14**	117.6(2)	124.8(3)
C15–N16–C17	124.0(2)	122.3(2)	**C15–N16–C24**	124.4(2)	124.6(2)
C17–N16–C24	111.5(2)	111.8(3)			
C7–C6–N1–C10	3.2(3)	−0.4(5)	**C6–C7–C8–C9**	−57.7(3)	−61.8(4)
C7–C8–C9–C10	68.3(3)	63.6(4)	**C8–C9–C10–N1**	−43.3(3)	−33.5(5)
C9–C10–N1–C6	7.5(3)	1.4(5)	**C7–C8–C9–C11**	−59.0(3)	−61.0(4)
C8–C9–C11–N12	49.6(3)	57.2(4)	**C9–C11–N12–C13**	−45.0(3)	−53.0(5)
C11–N12–C13–C7	49.6(3)	52.2(4)	**N12–C13–C7–C8**	−60.2(3)	−56.3(4)
C13–C7–C8–C9	64.8(3)	60.8(4)	**C9–C11–N12–C14**	154.7(2)	147.9(4)
C7–C13–N12–C14	−148.9(2)	−150.6(3)	**C11–N12–C14–C15**	−13.1(3)	177.9(3)
C13–N12–C14–C15	−173.1(2)	21.1(4)	**N12–C14–C15–N16**	−176.7(2)	60.4(3)
C11–N12–C14–O14	167.2(2)	−2.6(5)	**C13–N12–C14–O14**	7.2(4)	−159.4(3)
C14–C15–N16–C17	−77.6(3)	99.2(3)	**C14–C15–N16–C24**	97.4(3)	57.9(4)

It might be noted that in nine N-carbonyl cytisine derivatives deposited in the CSD [31], only in one case (carbamide, 6-oxo-7,11-diazatricyclo[7.3.1.02,7]trideca-2,4-diene-11-carboxamide [32]) the conformation of C=O bond is anti with respect to C11–N12 bond (as in 1), while in the other eight cases the conformation is syn, like in 2, with the mean value of C11–N12–C14–O14 torsion angle at 2.2(19)°.

3.1. The Importance of the Quality of the Electron Density Model

Three different models of electron density distribution were tested:

(a) original X-ray independent atom model (IAM-standard model of X-ray structure determination);

(b) IAM model with hydrogen atoms moved to the average geometries determined by means of neutron diffraction; and

(c) The model with geometry as in (b) but upgraded to the multipolar level [33] by transferring the coefficients of multipolar expansion from the ELMAM2 database [34], (except for the cyan group, for which the parameters were transferred from the published molecule of [35] due to the absence in ELMAM2).

It turned out that the results obtained in the latter two approaches for intermolecular contacts were quite similar in terms of both critical points positions and their characteristics, but the results for intramolecular bonds showed obvious advantages of transferring procedure, especially for polarized C=O bonds.

To have deeper insight into this, we compared the topological parameters of the covalent bonds with those obtained experimentally, by means of high-resolution diffraction studies, for similar compounds: (–)-cytisine and N-methyl-cytisine [36]. The results of such comparison for selected bonds are presented in Figure 5 for electron density value at the critical point and for Laplacian value. The results for all bonds between non–H atoms are submitted as supplementary materials.

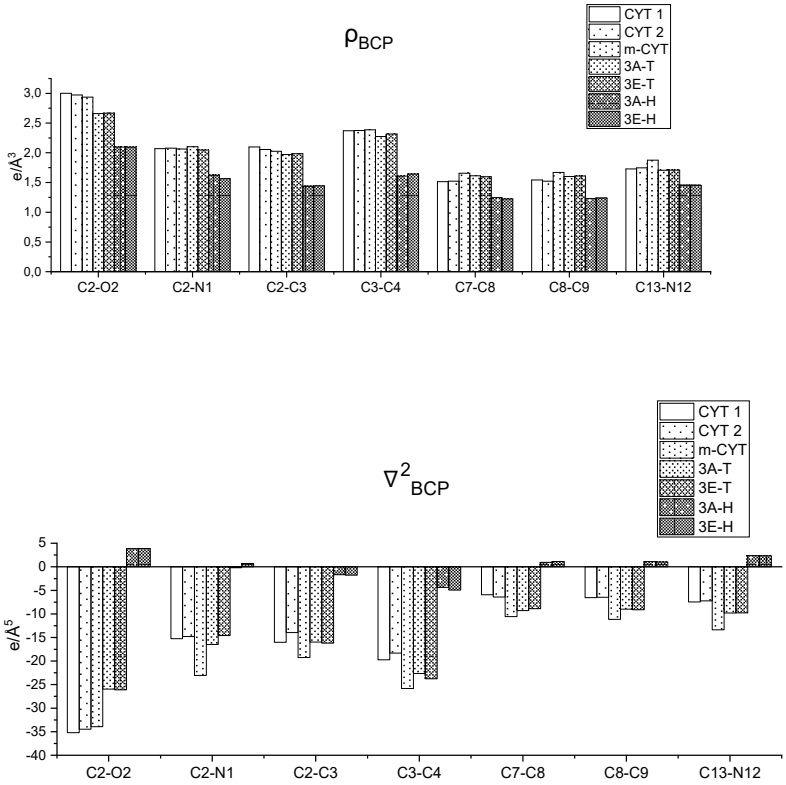

Figure 5. A comparison of the values of electron density at bond critical point (top) and Laplacian (bottom) at this point. The codes are: CYT1, CYT2–two symmetry independent molecules of (-)cytisine [19], m-CYT—*N*-methylcytisine [19], 3A-T, 3E-T: molecules **3A** and **3E** with transferred multipolar coefficients; 3A–H, 3E–H: **3A** and **3E** at IAM level with H atoms moved to neutron positions.

The results show clearly that the transfer of multipolar parameters improves the quality of the electron density maps. It is especially obvious for Laplacian values, where for most of the bonds even the sign is incorrect. It might be noted also that the distances between atoms, and in general geometries of the cytisine skeletons were almost identical in all studied cases.

3.2. Crystal Packing, Intermolecular Interactions

Due to the absence of strong hydrogen bond donors, charged species and halogen atoms, the crystal architecture is determined by a number of weak interatomic interactions. Here we are going to show the comparison between different approaches: geometrical, energy calculations and topological analysis.

The most important interactions can be conveniently identified by means of Hirshfeld surface analysis [37], which allows one to visualize the regions of the molecule under consideration with the closest contacts (in the terms of van der Waals radii) with neighboring molecules.

In such a way, the closest (as compared to sums of van der Waals radii) intermolecular contacts have been found and then each of them analyzed (Figure 6).

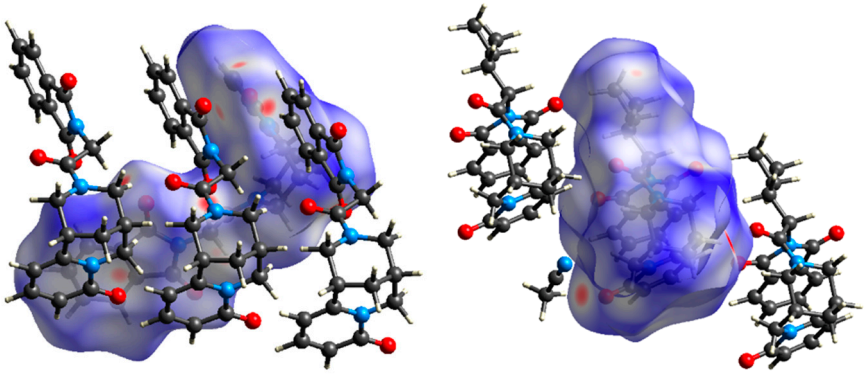

Figure 6. Hirshfeld surfaces of molecules **3A** (left) and **3E** (right) with the closest neighbors.

In *N*-[glycine-(*N*-phtaloyl)]cytisine (**1**), the most pronounced contact is related with the C9–H9···O14 (−1 + x,y,z) weak hydrogen bond, with the shortest H···O distance (2.45 Å), which connects the molecules into infinite chains along the x direction. It is also the interaction which defines two molecules with the highest interaction energy, calculated at −51.8 kJ/mol by B3LYP and at −55.3kJ/mol by the PIXEL method (cf. experimental part). The critical point found for this interaction is also described by the highest values of electron density (0.092/0.072 e/Å^3; hereinafter the first value is obtained for the IAM model with elongated C–H bonds, and the second one with the model with transferred multipole parameters; cf. Experimental part) and Laplacian (1.099/1.090 e/Å^5) at the CP. The second shortest H···O distance was found for H15A···O24 (−1/2 + x, 3/2−y, −z), and for these two molecules also the second-highest energies (−43.0/−40.9 kJ/mol) and the critical point of second-highest electron density (0.078/0.065) and Laplacian (0.939/0.771) were calculated. More details can be found in Table 3; here, we would like to show examples for which differences between DFT (B3LYP) and PIXEL methods are significant. For two molecules connected by weak H21···O2 (3/2 + x,3/2 − y, −z), with the H···O distance of 2.59Å, the interaction energy calculated with the first method is −17.8 kJ/mol, while with the second one it is −9.2 kJ/mol. For this interaction, well-defined critical points with one of the highest characteristics (0.076/0.059 and 0.910/0.718) were found.

Additionally, in *N*-[*L*-isoleucine-(*N*-phtaloyl)]cytisine (**2**), the shortest C–H···O contact (H5·· O14, 2.38 Å), again between the molecules related by unique translation along x, is connected with the highest interaction energy (−44.2/−45.8 kJ/mol). The characteristics of the appropriate bond critical point (0.119/0.093, 1.363/1.169) indicate the strongest interaction. Energetically comparable is the interaction between molecules related by y

unit-cell translation, although related with longer H13A···O2 contact of 2.65 Å. The energies calculated for this pair are −41.7 and −35.6 kJ/mol for DFT (B3LYP) and PIXEL methods, respectively. This energy is significantly larger than that calculated for apparently shorter contact, H3A2···O2 (2.45 Å): −26.8/−9.3 kJ/mol. Interestingly enough, both the electron density and Laplacian values at the appropriate critical points have the higher values for the latter contact (0.096/0.075 and 1.127/0.909) than for the former one (0.061/0.042 and 0.757/0.731).

The explanation of such discrepancies lies probably in the number of interactions (or contacts) between the molecules, as the overall interaction energies consider all these interactions, even very weak ones. For instance, taking the strongest intermolecular interactions in 1, this between molecules at (x,y,z) and (−1 + x,y,z), there are eight contacts for which critical points were found. The results for this contact are presented in Figure 7 and Table 4. The full set of such comparisons is submitted as supplementary information.

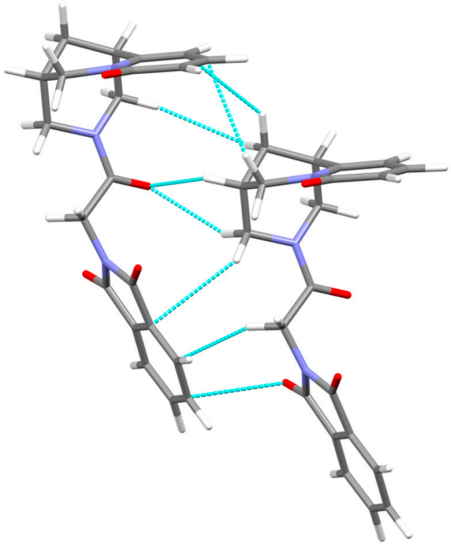

Figure 7. An example of a pair of molecules (related by unit translation along the x-direction) and connected by weak, numerous interactions, giving rise to relatively high interaction energy: Eint: −51.8 kJ/mol (B3LYP); −55.3 kJ/mol (PIXEL).

Similarly, for **2**, the highest energy was found for the pair of molecules, for which as many as 10 contact critical points were found (Figures 7 and 8, Table 5).

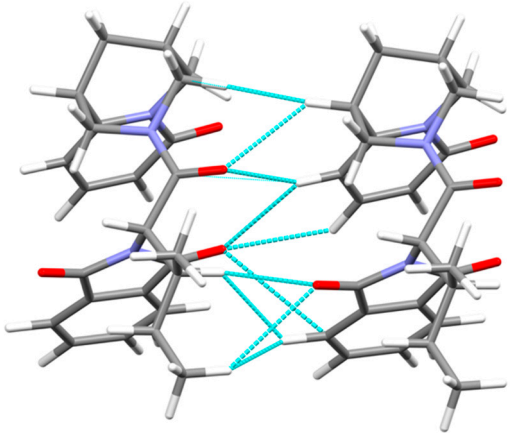

Figure 8. An example of a pair of molecules (related by unit translation along x-direction) and connected by weak, numerous interactions, giving rise to relatively high interaction energy: E_{int}: −44.2 kJ/mol (B3LYP); −43.3 kJ/mol (PIXEL).

Table 4. The details of the interactions for the pair of the highest interaction energy in 1 ($^{i:}$ −1+x, y, z: 8 contacts with critical points). Upper part: geometrical details; lower: topological; D12: distance between two atoms; Gcp: kinetic energy density (kJ/mol/Bohr3); Vcp: potential energy density (kJ/mol/Bohr^3); Dcp1, Dcp2: distance from the first and the second atom to the critical point, respectively; Lap: laplacian [$\nabla^2(\rho_{bcp})$ (eÅ^{-5})]; Den: electron density [ρ_{bcp} (eÅ^{-3})].

D	**H**	**A**	**D–H**	**H···A**	**D···A**	**D–H···A**
C9	H9	O14^i	1.09	2.39	3.181	129
C15	H15B	C22^i	1.09	2.73	3.896	117
C11	H11B	O14^i	1.09	2.61	3.310	122
C8	H8B	C5^i	1.09	3.31	3.854	144
C10	H10A	C4^i	1.09	2.99	3.963	150
C11	H11A	C23^i	1.09	3.14	3.896	127
			contacts			
O17	C20^i				3.826	
H8A	H13B^i				2.90	

Atom 1	**Atom 2**	**Gcp**	**Vcp**	**D12**	**Dcp1**	**Dcp2**	**Den**	**Lap**
H9	O14^i	23.65	−17.62	2.3798	0.9848	1.3951	0.072	1.09
H15B	C22^i	15.46	−11.13	2.7260	1.0967	1.6605	0.052	0.727
H11B	O14^i	14.63	−9.44	2.6056	1.1224	1.5003	0.039	0.727
H8B	C5^i	7.76	−5.04	2.9847	1.1959	1.8014	0.027	0.385
H10A	C4^i	5.61	−3.91	2.9823	1.2298	1.7607	0.026	0.269
H11A	C23^i	6.2	−3.91	3.1346	1.2537	1.9289	0.022	0.312
O17	C20^i	5.48	−3.46	3.5235	1.7248	1.8222	0.020	0.275
H8A	H13B^i	2.88	−1.72	2.8997	1.4358	1.4647	0.012	0.149

Table 5. The details of the interactions for the pair of the highest interaction energy in **2** (^{i} 1+x, y, z: 10 contacts with critical points). Upper part: geometrical details; lower: topological; D12: distance between two atoms; Gcp: kinetic energy density (kJ/mol/Bohr3); Vcp: potential energy density (kJ/mol/Bohr^3); Dcp1, Dcp2: distance from the first and the second atom to the critical point, respectively; Lap: laplacian [$\nabla^2(\rho_{bcp})$ (eÅ^{-5})]; Den: electron density [ρ_{bcp} (eÅ^{-3})].

D	**H**	**A**	**D–H**	**H···A**	**D···A**	**D–H···A**
C5	H5	O14^i	1.09	2.23	3.257	157
C7	H7	O14^i	1.09	2.65	3.798	136
C25^i	H25^i	O17	1.09	2.72	3.537	132
C4	H4	O24^i	1.09	2.81	3.551	125
C5	H5	O24^i	1.09	2.86	3.566	123
C28^i	H28B^i	O17	1.09	3.04	3.913	138
			contacts			
C19	O24^i				3.526	
H19	H25				2.558	
H19	H28B				2.605	
H7	H11A^i				2.459	

Table 5. *Cont.*

Atom 1	Atom 2	Gcp	Vcp	D12	Dcp1	Dcp2	Den	Lap
H5	O14	27.12	−22.4	2.2334	0.8943	1.3399	0.093	1.169
H7	O14	11.61	−7.79	2.6429	1.1201	1.5251	0.038	0.566
O17	H25	10.21	−6.68	2.7114	1.5597	1.153	0.033	0.505
H7	H11A	5.72	−4.09	2.4475	1.2347	1.2151	0.028	0.27
H4	O24	7.83	−4.76	2.8178	1.2065	1.6115	0.023	0.4
H5	O24	7.32	−4.43	2.8605	1.2263	1.636	0.021	0.375
C19	O24	5.83	−3.56	3.5262	1.8699	1.6669	0.019	0.297
H19	H25	5.44	−3.36	2.5544	1.2681	1.2919	0.019	0.276
H19	H28B	4.47	−2.71	2.6173	1.3034	1.3178	0.016	0.229
O17	H28B	4.34	−2.65	3.0464	1.7272	1.3338	0.016	0.222

4. Conclusions

Eight new derivatives of (–)-cytisine, an alkaloid of biological importance, were synthesized and fully spectroscopically analyzed (NMR, FTIR). The general formula of the new compounds is (–)-(*N*-[(amino acid)-(*N*-phtaloyl)]cytisine. Mass spectrometry was used for proposing the fragmentation routes of new compounds. For two derivatives, namely glycine and L-isoleucine derivatives, the X-ray crystal structures were determined and used for in-depth analysis of intermolecular interactions, based on geometries of the structures, quantum chemical calculations of interaction energies, and characterization of the critical points of the electron density distribution based on atoms-in-molecules theory. No direct and strict correlation between the geometrical characteristics (distances, even angles) of the interaction and the energetical or topological parameters could be found. Instead, the results suggest that the interaction energies are correlated with the number of contacts and of critical points between molecules, rather in line with the reasoning of Dunitz and Gavezzotti [38]. Additionally, by comparing the results of the topological analysis with those obtained for cytisine and *N*-methyl cytisine by means of experimental method (high-resolution diffraction), the importance of the transfer of multipolar parameters was shown—only such a model was able to give results similar to the experimental ones.

Supplementary Materials: The following are available online at https://www.mdpi.com/2073-4352/11/2/146/s1: Table S1: FTIR–characteristic bands for compounds **3** [cm^{-1}]; Figures. S1–S39: GC-MS, EI-MS, FTIR ^{13}V NMR spectra for compounds **3A**–**3F**. Tables S2 and S3: Intermolecular interaction details for **3A** and **3E**.

Author Contributions: Conceptualization, A.K.P. and M.K.; methodology, A.K.P., A.M.G., M.K.; software, A.M.G., M.K.; validation, A.M.G., M.K.; investigation, A.K.P., A.M.G., M.K.; resources, M.K.; writing—original draft preparation, A.K.P., M.K.; writing—review and editing, A.K.P., M.K.; visualization, A.K.P., A.M.G., M.K.; supervision, A.K.P., M.K..; project administration, M.K.; funding acquisition, M.K. All authors have read and agreed to the published version of the manuscript.

Funding: This research was funded by National Science Center (Poland) project (Grant No. 2013/11/B/ST5/01681).

Institutional Review Board Statement: Not applicable.

Informed Consent Statement: Not applicable.

Data Availability Statement: Crystallographic data for the structural analysis has been deposited with the Cambridge Crystallographic Data Centre, Nos. CCDC–1851176 (**1**) and 1851175 (**2**). Copies of this information may be obtained free of charge from: The Director, CCDC, 12 Union Road, Cambridge, CB2 1EZ, UK. Fax: +44(1223)336-033, e-mail: deposit@ccdc.cam.ac.uk, or www: www.ccdc.cam.ac.uk.

Conflicts of Interest: The authors declare no conflict of interest. The funders had no role in the design of the study; in the collection, analyses, or interpretation of data; in the writing of the manuscript, or in the decision to publish the results.

References

1. Dunitz, J.D. Phase transitions in molecular crystals from a chemical viewpoint. *Pure Appl. Chem.* **1991**, *63*, 177–185. [CrossRef]
2. Lehn, J.-M. From supramolecular chemistry towards constitutional dynamic chemistry and adaptive chemistry. *Chem. Soc. Rev.* **2007**, *36*, 151–160. [CrossRef] [PubMed]
3. Desiraju, G.R. The C-H···O hydrogen bond: Structural implications and supramolecular design. *Acc. Chem. Res.* **1996**, *29*, 441–449. [CrossRef] [PubMed]
4. Cavallo, G.; Metrangolo, P.; Milani, R.; Pilati, T.; Priimagi, A.; Resnati, G.; Terraneo, G. The halogen bond. *Chem. Rev.* **2016**, *116*, 2478–2601. [CrossRef]
5. Scilabra, P.; Terraneo, G.; Resnati, G. The chalcogen bond in crystalline solids: A world parallel to halogen bond. *Acc. Chem. Res.* **2019**, *52*, 1313–1324. [CrossRef] [PubMed]
6. Scheiner, S. The pnicogen bond: Its relation to hydrogen, halogen, and other noncovalent bonds. *Acc. Chem. Res.* **2020**, *46*, 280–288. [CrossRef]
7. Bauza, A.; Mooibroek, T.J.; Frontera, A. Tetrel-Bonding interacion: Rediscovered supramolecular force? *Angew. Chem. Int. Ed.* **2013**, *52*, 12317–12321. [CrossRef]
8. Thakuria, R.; Nath, N.K.; Saha, B.K. The nature and applications of π···π interactions: A perspective. *Cryst. Growth Des.* **2019**, *19*, 5230528. [CrossRef]
9. Mahadevi, A.S.; Sastry, N. Cation-π interaction: Its role and relevance in chemistry, biology, and material science. *Chem. Rev.* **2013**, *113*, 2100–2138. [CrossRef]
10. Wang, D.-X.; Wang, M.-X. Anion-π interactions: Generality, binding strength, and structure. *J. Am. Chem. Soc.* **2013**, *135*, 892–897. [CrossRef]
11. Tutka, P.; Zatoński, W. Cytisine for the treatment of nicotine addiction: From a molecule to therapeutic efficiacy. *Pharmacol. Rep.* **2005**, *58*, 777–798.
12. Rouden, J.; Lasne, M.-C.; Blanchet, J.; Baudoux, J. (−)-Cytisine and derivatives: Synthesis, reactivity, and applications. *Chem. Rev.* **2014**, *114*, 712–778. [CrossRef] [PubMed]
13. Kozikowski, A.P.; Chellappan, S.K.; Xiao, Y.; Bajjuri, K.M.; Yuan, H.; Kellar, K.J.; Petukhov, P.A. Chemical medicine: Novel 10-substituted cytisine derivatives with increased selectivity for α4β2 nicotinic acetylcholine receptors. *ChemMedChem* **2007**, *2*, 1157–1161. [CrossRef] [PubMed]
14. Artyushin, O.I.; Moiseeva, A.A.; Zarubaev, V.V.; Slita, A.V.; Galochkina, A.V.; Muryleva, A.A.; Borisevich, S.S.; Yarovaya, O.I.; Salakhutdinov, N.F.; Brel, V.K. Synthesis of camphecene and cytisine conjugates using click chemistry methodology and study of their antiviral activity. *Chem. Biodivers.* **2019**, *16*, e1900340. [CrossRef] [PubMed]
15. Bhat, S.V.; Nagasampagi, B.A.; Sivakumar, M. *Chemistry of Natural Products*; Springer: Berlin/Heidelberg, Germany, 2005; pp. 237–315.
16. Juaristi, E.; Beck, A.K.; Hansen, J.; Matt, T.; Mukhopadhyay, T.; Simson, M.; Seebach, D. Enantioselective aldol and Michael additions of achiral enolates in the presence of chiral lithium amides and amines. *Synthesis* **1993**, *1993*, 1271–1290. [CrossRef]
17. Kánai, K.; Podányi, B.; Bokotey, S.; Hajdú, F.; Hermecz, I. Stereoselective sulfoxide formation from a thioproline derivative. *Tetrahedron Asymmetry* **2002**, *13*, 491–496. [CrossRef]
18. Przybył, A.K.; Prukała, W.; Kikut-Ligaj, D. EI-MS study of selected N-amide and N-alkyl derivatives of cytisine. *Rapid Commun. Mass Spectrom.* **2007**, *21*, 1409–1413. [CrossRef]
19. Przybył, A.K.; Nowakowska, Z. EIMS study of Halogenated N-Acetyl- and N-Propionylcytisines. *Rapid Commun. Mass Spectrom.* **2011**, *25*, 1193–1197. [CrossRef]
20. Przybył, A.K.; Kubicki, M. A comparative study of dynamic NMR spectroscopy in analysis of selected N-alkyl-, N-acyl-, and halogenated cytisine derivatives. *J. Mol. Struct.* **2011**, *985*, 157–166. [CrossRef]
21. Przybył, A.K.; Kubicki, M.; Hoffmann, M. The amide protonation of (-)-N-benzoyl-cytisine in its perchlorate salts. *Spectrochim. Acta A Mol. Biomol. Spectr.* **2014**, *129*, 1–6. [CrossRef]
22. *CrysAlisPro*; Rigaku Oxford Diffraction LTd.: Oxford, UK, 2013.
23. Sheldrick, G.M. SHELXT—Integrated space-group and crystal-structure determination. *Acta Cryst. Part A* **2015**, *71*, 3–8. [CrossRef] [PubMed]
24. Sheldrick, G.M. Crystal structure refinement with SHELXL. *Acta Cryst. Part C* **2015**, *71*, 3–8. [CrossRef] [PubMed]
25. Turner, M.J.; McKinnon, J.J.; Wolff, S.K.; Grimwood, D.J.; Spackman, P.R.; Jayatilaka, D.; Spackman, M.A. CrystalExplorer17. University of Western Australia. 2017. Available online: http://crystalexplorer.scb.uwa.edu.au/ (accessed on 29 January 2021).
26. Gavezzotti, A. Are crystal structures predictable? *Acc. Chem. Res.* **1994**, *27*, 309–314. [CrossRef]
27. Gavezzotti, A.; Fillippini, G. Geometry of the intermolecular X-H···Y (X, Y = N, O) hydrogen bond and the calibration of empirical hydrogen-bond potentials. *J. Phys. Chem.* **1994**, *98*, 4831–4837. [CrossRef]
28. Macrae, C.F.; Sovago, I.; Cottrell, S.J.; Galek, P.T.A.; McCabe, P.; Pidcock, E.; Platings, M.; Shields, G.P.; Stevens, J.S.; Towler, M.; et al. Mercury 4.0: From visualization to analysis, design and prediction. *J. Appl. Cryst.* **2020**, *53*, 226–235. [CrossRef]

29. Bader, R.F.W. *Atoms in Molecules: A Quantum Theory*; Clarendon Press: Oxford, UK, 1990.
30. Guillot, B.; Viry, L.; Guillot, R.; Lecomte, C.; Jelsch, C. Refinement of proteins at subatomic resolution with MOPRO. *J. Appl. Cryst.* **2001**, *34*, 214–223. [CrossRef]
31. Groom, C.R.; Bruno, I.J.; Lightfoot, M.P.; Ward, S.C. The cambridge structural database. *Acta Cryst. Part B* **2016**, *72*, 171–179. [CrossRef]
32. Suponitskii, K.Y.; Tsypysheva, I.P.; Kovalskaya, A.V. Molecular and crystal structure of (1R,5S)-8-oxo-1,5,6,8-tetrahydro-2H-1,5-methanopyrido[1,2-a][1,5]diazocine-3(4H)-carboxamide and (1R,5S)-8-OXO-1,5,6,8-tetrahydro-2H-1,5-methanopyrido[1,2-a][1,5]diazocine-3(4H)-thiocarbo-xamide. *J. Struct. Chem.* **2015**, *56*, 188–190. [CrossRef]
33. Hansen, N.; Coppens, P. Testing aspherical atom refinements on small-molecule data sets. *Acta Cryst. Part A* **1978**, *71*, 3–8. [CrossRef]
34. Domagala, S.; Fournier, B.; Liebschner, D.; Guillot, B.; Jelsch, C. An improved experimental databank of transferable multipolar atom models—ELMAM2. Construction details and applications. *Acta Cryst. Part A* **2012**, *68*, 337–351. [CrossRef]
35. Paul, A.; Kubicki, M.; Kubas, A.; Jelsch, C.; Fink, K.; Lecomte, C. Charge density analysis of 2-methyl-4-nitro-1-phenyl-1H-imidazole-5-carbonitrile: An experimental and theoretical study of C≡N ···C≡N interactions. *J. Phys. Chem. A* **2011**, *115*, 12941–12952. [CrossRef] [PubMed]
36. Owczarzak, A.; Grześkiewicz, A.M.; Kubicki, M. Experimental studies of charge density distribution in the crystals of cytisine and N-methylcytisine. Inside the fake tobacco. *Struct. Chem.* **2017**, *28*, 1359–1367. [CrossRef]
37. McKinnon, J.J.; Spackman, M.A.; Mitchell, A.S. Hirshfeld surfaces: A new tool for visualizing and exploring molecular crystals. *Chem. Eur. J.* **1998**, *4*, 2136–2141. [CrossRef]
38. Dunitz, J.D.; Gavezzotti, A. Molecular recognition in organic crystals. Directed intermolecular bonds or nonlocalized bonding? *Angew. Chem. Int. Ed.* **2005**, *44*, 1766–1787. [CrossRef]